

ON THE STABILITY OF PROTON BEAMS AGAINST RESONANT SCATTERING BY ALFVÉN WAVES IN SOLAR FLARE LOOPS

DAVID H. TAMRES¹

Department of Physics, University of California at San Diego

D. B. MELROSE

School of Physics, University of Sydney

AND

RICHARD C. CANFIELD²

Institute for Astronomy, University of Hawaii
 Received 1987 June 8; accepted 1988 December 14

ABSTRACT

The passage of an energetic population of charged particles through a flaring coronal loop may, depending upon conditions, drive the growth of Alfvén waves in the ambient plasma. After an increase of several e -foldings in wave energy density, resonant scattering begins to reduce significantly the anisotropy of the particles driving the wave growth. In the present paper we assess the velocity-space stability of a steady state, sub-MeV proton beam in a solar flare loop by considering the conditions for the effective growth of Alfvén waves.

We determine the growth of Alfvén waves in a magnetized hydrogen plasma at flare loop densities and magnetic field strengths using quasi-linear theory. Wave-particle resonant interactions are calculated at the harmonics $s = 0, \pm 1, \pm 2$, and so on, until convergence is achieved in the growth rate to a tolerance of 1%. The dilute proton beam driving the wave growth is parameterized in terms of the characteristic speed v_o and the median pitch angle α_{50} of the distribution. Two cases of beam energy are considered: in the first, v_o is set equal to the Alfvén speed v_A in order to model a beam whose mean energy lies in the deka-keV range; in the second, the mean energy is one order of magnitude larger ($v_o = 10^{1/2}v_A$). The effect of beam collimation on wave growth is investigated by varying α_{50} over a range extending from 8° (strong collimation) to 60° (mild collimation). The dependence of the growth rate on frequency and wave angle is presented and discussed.

To assess the stability of the beam, we compare the loop semilength L to the length scale for effective wave growth L_G . Explicitly included in the determination of L_G , in addition to the beam-driven growth, is the thermal damping that results from the resonant interaction between Alfvén waves and the thermal background. Beam stability is defined in the present context by the condition $L_G > L$, which can be recast as an upper limit on the beam-to-background proton density ratio n^*/n_i corresponding to a given value of α_{50} . The variation of this upper limit with respect to α_{50} , and the effectiveness of thermal damping in relaxing this upper limit, is presented.

We find that under typical flare conditions ($B = 10^2$ G, $n_i = 10^{10}$ cm⁻³, $T =$ a few million K, loop semilength $L = 10^9$ cm) thermal damping in the case $v_o = v_A$ effectively stabilizes proton beams of moderate collimation ($\alpha_{50} \gtrsim 40^\circ$). By contrast, at beam energies only one order of magnitude larger, thermal damping under flare loop conditions is insufficient to prevent highly restrictive upper limits on the beam-to-background proton density ratio for even mildly collimated proton beams. We conclude that streaming instabilities begin to pose serious constraints on the sustained propagation of directed proton streams in solar flare loops at energies that are only a small multiple of $m_p v_A^2/2$.

Subject headings: instabilities — plasmas — Sun: corona — Sun: flares — wave motions

I. INTRODUCTION

McClements (1987) and Mok (1985) have examined the microscopic stability of deka-keV electrons streaming through flaring coronal loops. In a similar spirit, we address the microscopic stability of streaming protons of energy 10–1000 keV in the same environment. Protons may achieve these and higher energies in flares as a result of shock acceleration, stochastic acceleration, or acceleration in direct electric fields (Forman, Ramaty, and Zweibel 1986 and references therein). High-energy ($E > 2$ MeV) protons at the flare site have been identified by means of their radiative signature in gamma-rays (see discussions of solar gamma-ray line emission by, e.g., Chupp *et*

al. 1973; Ramaty, Kozlovsky, and Lingenfelter 1975; Chupp 1984). Flare-associated protons of lower energy have been detected by satellites in the interplanetary medium (e.g. Sarris and Krimigis 1985) but the interpretation of their spectra is complicated by the need to account for the interplanetary magnetic field geometry, the interaction with the solar wind, and the acceleration of protons at shock fronts in interplanetary space. There is considerable interest in identifying a radiative signature of sub-MeV protons at the flare site (Benz and

¹ Also Institute for Astronomy, University of Hawaii.

² Also Department of Physics, University of California at San Diego.

Simnett 1986; Tamres, Canfield, and McClymont 1986; Canfield and Chang 1985; Orrall and Zirker 1976) and thus motivation for understanding the important physical processes associated with these particles in the flare environment. This includes an understanding of the limitations imposed by streaming instabilities on the propagation of a directed, superthermal distribution (i.e., a "beam") of protons in a flare loop.

Our goal is to assess the conditions for the effective scattering of a proton beam through resonant interaction with waves in the background plasma—waves that have themselves been driven to growth through resonant interaction with the fast protons. For effective resonant scattering of fast protons, the relevant wave modes are the Alfvén mode and the magnetoacoustic mode (Melrose 1986). In the present study we consider only the Alfvén mode. In § II, we present the method by which we calculate the quasi-linear growth of Alfvén waves driven by a beam of sub-MeV protons. The dependence of this growth on wave frequency and wave angle is discussed in § III. Also in § III we introduce thermal damping and discuss its influence on beam stability in the flare loop. Our conclusions are stated in § IV.

To limit the scope of the study and to reduce the degree of mathematical and computational complexity, we have incorporated several idealizations and approximations. We represent the background medium as a pure hydrogen plasma, thereby precluding additional wave damping due to the presence of helium and other heavy ions. The dimensionality of the problem is kept to a minimum by restricting the calculation to instantaneous measures of wave growth in a homogeneous medium; consequently, we do not follow the spatial and temporal evolution of the proton distribution. Regarding temperature effects, we include wave damping due to resonant interaction involving particles of the thermal background but do not introduce thermal corrections into the cold-plasma dispersion relation. The dispersion relation is also uncorrected for the presence of the dilute beam. The nonuniform topology of the background magnetic field is ignored, as are nonlinear processes. Only resonant-type instabilities are considered. Finally, we assume that the mechanism energizing the protons and giving rise to the distribution that drives the wave growth is continuously operative for a duration longer than the time required for the driven waves to propagate a distance equal to one length scale of growth (that is, energization time scale $> L_G/v_{g\parallel}$, where $v_{g\parallel}$ is the parallel component of the group velocity of the most vigorously growing waves). This implies energization time scales as long as several seconds. Whether this corresponds to the actual situation in the flare environment is unknown. If wave growth is not continuously driven (if, for example, proton energization is a pulsed, rather than a continuous, process), beam stability is expected to be greater than that implied by the criterion we derive below.

II. WAVE-PARTICLE INTERACTION

a) Formalism

A semiclassical treatment of wave-particle interactions in a magnetized plasma may be found, e.g., in the work of Melrose (1980), where it is shown that the quasi-linear absorption coefficient $\gamma^\sigma(\mathbf{k})$ describing the effects of induced processes on the distribution of waves in the mode σ takes the form

$$\gamma^\sigma(\mathbf{k}) = -\sum_a \sum_{s=-\infty}^{\infty} \int d^3p w_a^\sigma(s, \mathbf{p}, \mathbf{k}) \hbar \left(\frac{s\Omega_a}{v_\perp} \frac{\partial}{\partial p_\perp} + k_\parallel \frac{\partial}{\partial p_\parallel} \right) f_a(\mathbf{p}). \quad (1)$$

The absorption coefficient $\gamma^\sigma(\mathbf{k})$ is related to the wave occupation number $N^\sigma(\mathbf{k})$ according to $dN^\sigma(\mathbf{k})/dt = -\gamma^\sigma(\mathbf{k})N^\sigma(\mathbf{k})$, so that negative values of $\gamma^\sigma(\mathbf{k})$ correspond to growth rates. In equation (1), the subscripts \parallel and \perp , respectively, denote the parallel and perpendicular components of vector quantities with respect to the ambient magnetic field, $f_a(\mathbf{p})$ is the momentum-space distribution function of species a , \mathbf{k} denotes the wavevector, \hbar is the Planck constant over 2π , Ω_a denotes the (relativistic) gyrofrequency of species a , and

$$w_a^\sigma(s, \mathbf{p}, \mathbf{k}) = \frac{8\pi^2 q_a^2 R_E^\sigma(\mathbf{k})}{\hbar \omega^\sigma(\mathbf{k})} \times |\hat{\mathbf{e}}^{\sigma*}(\mathbf{k}) \cdot \mathbf{V}_a(s, \mathbf{p}, \mathbf{k})|^2 \delta(\omega^\sigma(\mathbf{k}) - s\Omega_a - k_\parallel v_\parallel), \quad (2)$$

where q_a is the electric charge of particles of species a . Both the Dirac δ -function in equation (2), which expresses the Doppler condition for wave-particle resonance, and the vector $\mathbf{V}_a(s, \mathbf{p}, \mathbf{k})$ formally originate from the spatial and temporal Fourier transform of the current associated with spiraling charged particles in a magnetic field. The latter has the form

$$\mathbf{V}_a(s, \mathbf{p}, \mathbf{k}) = \left[\frac{s}{\zeta_a} v_\perp J_s(\zeta_a), -i \frac{q_a}{|q_a|} v_\perp J'_s(\zeta_a), v_\parallel J_s(\zeta_a) \right], \quad (3)$$

$$\zeta_a = \frac{k_\perp v_\perp}{\Omega_a}$$

in a coordinate system in which the unit vector $\hat{\mathbf{z}}$ points along the ambient magnetic field, $\hat{\mathbf{y}}$ points along $\mathbf{B} \times \mathbf{k}$, and $\hat{\mathbf{x}} = \hat{\mathbf{y}} \times \hat{\mathbf{z}}$. In equation (3), J_s denotes the Bessel function of the first kind of order s , and a prime on J_s denotes differentiation with respect to the argument. The quantities $\hat{\mathbf{e}}^{\sigma*}(\mathbf{k})$ and $R_E^\sigma(\mathbf{k})$ in equation (2) describe wave properties: $\hat{\mathbf{e}}^{\sigma*}(\mathbf{k})$ is the complex conjugate of the electric polarization unit vector and $R_E^\sigma(\mathbf{k})$ is the ratio of electric energy density to total energy density in the wave (see Appendix).

The dispersion relation for waves in a charge-neutral, magnetized cold plasma of fully ionized hydrogen may be written as a quadratic equation in n^2 , where n is the refractive index ($n^2 = c^2 k^2 / \omega^2$). For wave frequencies less than, but not necessarily a small fraction of, the proton gyrofrequency Ω_i , this quadratic equation takes the form (Stix 1962, chap. 2, eq. [28])

$$n^4 \cos^2 \theta - n^2 \frac{c^2}{v_A^2(1-\chi^2)} (1 + \cos^2 \theta) + \frac{c^4}{v_A^4(1-\chi^2)} = 0, \quad (4)$$

$$\chi = \frac{\omega}{\Omega_i},$$

provided that the wave angle θ ($= \cos^{-1}(k_\parallel/|\mathbf{k}|)$) lies outside the immediate vicinity of $\pi/2$ and that $c^2 \gg v_A^2$, where c is the speed of light and v_A is the Alfvén speed [$= B/(4\pi n_i m_p)^{1/2}$]. Equation (4) has two solutions, one describing the fast mode (the magnetoacoustic mode) and the other describing the slow mode (the Alfvén mode). For the Alfvén mode, the solution is

$$n^2 = \frac{c^2}{2v_A^2(1-\chi^2)} [1 + \sec^2 \theta + (\tan^4 \theta + 4\chi^2 \sec^2 \theta)^{1/2}]. \quad (5)$$

For χ approaching unity from below, equation (5) describes ion cyclotron waves, while at the opposite limit (χ much less than unity), it yields the familiar dispersion relation for classic low-frequency Alfvén waves ($\omega^2 = k_\parallel^2 v_A^2$).

For the purpose of investigating a proton beam of sub-MeV

energies in a plasma at keV temperatures it suffices to consider the nonrelativistic limit of equation (1). One obtains

$$\gamma^\sigma(\mathbf{k}) = -\frac{16\pi^3 R_E^2(\mathbf{k})}{\omega^\sigma(\mathbf{k}) |k_\parallel|} \sum_a \frac{q_a^2}{m_a} \sum_{s=-\infty}^{\infty} \int_0^\infty dv_\perp v_\perp \times \left[|\hat{\mathbf{e}}^{\sigma*}(\mathbf{k}) \cdot \mathbf{V}_a(s, \mathbf{p}, \mathbf{k})|^2 \left(\frac{s\Omega_a}{v_\perp} \frac{\partial}{\partial v_\perp} + k_\parallel \frac{\partial}{\partial v_\parallel} \right) f_a(v) \right]_{v_\parallel = (\omega - s\Omega_a)/k_\parallel} \quad (6)$$

To represent a dilute population of fast, streaming protons in the system, we require a velocity distribution function whose essential characteristics are a superthermal mean speed and a preferential weighting of velocities in the streaming direction. A function with appropriate properties is

$$f(v) = \frac{n^*}{(2\pi v_o^2)^{3/2} Q(\beta)} e^{-v^2/2v_o^2} \times \begin{cases} 1 + (e^\beta - 1)e^{-\beta \tan^2 \alpha}, & 0 \leq \alpha < \frac{\pi}{2}, \\ 1, & \frac{\pi}{2} \leq \alpha \leq \pi, \end{cases} \quad (7)$$

where α is the pitch angle ($=\cos^{-1}(v_\parallel/|v|)$). The degree of anisotropy in this distribution is controlled by the parameter β . For $\beta = 0$, the distribution is a (dilute) isotropic Maxwellian characterized by a (superthermal) speed v_o . Larger values of β yield a velocity distribution more heavily weighted in the direction of the background magnetic field. It is more convenient for our discussion to describe the degree of anisotropy, not in terms of β , but rather in terms of the pitch angle α_{50} that marks the boundary of a cone in velocity space containing 50% of the particles described in equation (7). This angle is uniquely and monotonically related to the parameter β , and is defined formally by the relation

$$\frac{1}{n^*} \int_0^{\alpha_{50}} d\alpha \sin \alpha \int_0^\infty dv 2\pi v^2 f(v) = \frac{1}{2}. \quad (8)$$

The normalization factor $Q(\beta)$ in equation (7) ensures that the integral of $f(v)$ over velocity space yields n^* , the total number density of beam protons; $Q(\beta)$ is a monotonically increasing function of β that equals unity in the isotropic limit ($\beta = 0$) and behaves as $e^\beta/(4\beta)$ for $\beta \gg 1$.

b) Calculation Procedure

Equations (1) and (6) indicate that the absorption coefficient is formally the sum of an infinite number of integrals. Each of these integrals can itself be expressed in terms of an infinite series when $f(v)$ is taken to be of the form (7) (see Appendix). Where it proved feasible to carry out the series solution for individual integrals (generally, this requires $k_\perp v_o/\Omega_i$ to be less than or on the order of unity), the result was found to be in excellent agreement with the solution obtained by numerical integration. For values of $k_\perp v_o/\Omega_i$ notably larger than unity, individual integrals could only be evaluated by numerical integration. As a check against numerical instability, we carefully examined the behavior of the calculated integral over a wide range in $k_\perp v_o/\Omega_i$ and verified that it exhibited the expected asymptotic behavior when this parameter took on very large or very small values. Calculations were carried out on a Sun 3/260 workstation using double precision arithmetic. The numerical method for evaluation of integrals was Romberg

integration, described by Press *et al.* (1986); this reference also served as the source for the numerical methods used for evaluating Bessel and gamma functions. Spot checks of integrals in a later stage of the analysis using Simpson's rule provided further confidence in the accuracy of the integration procedure.

The absorption coefficient γ^σ was calculated on a set of grid points in (ω, θ) space. The grid in frequency consisted of the values $\omega/\Omega_i = 0.02, 0.04, \dots, 0.98$, while that in wave angle consisted of the values $\theta = 2^\circ, 4^\circ, \dots, 88^\circ$. For a given location on the grid, and for selected values of the parameters v_o and α_{50} , the absorption coefficient was calculated on the basis of equation (6), beginning the summation with the $s = 0$ term and proceeding to include higher order harmonics while monitoring the sum's convergence. The harmonics $s = 0, \pm 1, \pm 2$, and ± 3 were included as a matter of routine for every absorption coefficient calculated; higher order $\pm s$ pairs were incorporated as necessary until the sum had converged to within a tolerance of 1%. The incorporation of harmonics beyond $s = \pm 3$ proved necessary for convergence only in the regime of larger frequencies and wave angles, i.e., where $k_\perp v_o/\Omega_i$ is no longer small compared to unity. In the most demanding circumstances (large frequency, large wave angle, and large beam energy), convergence required between 40 and 50 harmonic pairs.

In view of the uncertainty regarding the precise physical conditions at the flare site, together with the uncertainty in the actual velocity-space distribution of energized protons during an event, our specification of 1% accuracy in the calculated growth rates may seem unnecessary. It is true that these uncertainties preclude anything more than an order-of-magnitude estimate of the overall wave growth rate. However, we have included as part of our goal an examination of how variations in the distribution function (i.e., variations in v_o and α_{50}) affect the patterns of wave growth in (ω, θ) space, in order that we may better understand the mechanisms of the streaming instability. For this, a relatively high accuracy in the computation of $\gamma^\sigma(\mathbf{k})$ is required in order that we may have confidence in the calculated patterns of wave growth.

III. DISCUSSION

a) Examination of the Growth Rate

Both the thermal and the nonthermal populations of charged particles contribute to the value of γ^σ . That equation (1) is linear in the distribution function allows us to consider these contributions separately. We discuss first the contribution from nonthermal protons and defer consideration of the thermal contribution to § IIIb.

We obtain the nonthermal contribution to γ^σ by identifying the distribution function in equation (6) with our chosen representation for a streaming population of protons, equation (7). The resulting expression for γ^σ is a function of the population parameters v_o and α_{50} and the wave parameters ω and θ . For our chosen representation for the nonthermal protons, wave growth does not occur for backward-propagating waves ($\cos \theta < 0$), hence it is necessary only to consider the forward propagation direction. Although alternative choices exist for the beam distribution function which may lead to some wave growth in the backward direction, one expects such wave growth to be weak in comparison to that in the forward direction. Relaxation of a streaming distribution involves the shedding of excess forward momentum, which is most effectively accomplished by the emission of forward-propagating rather than backward-propagating waves.

The behavior of the nonthermal contribution as a function

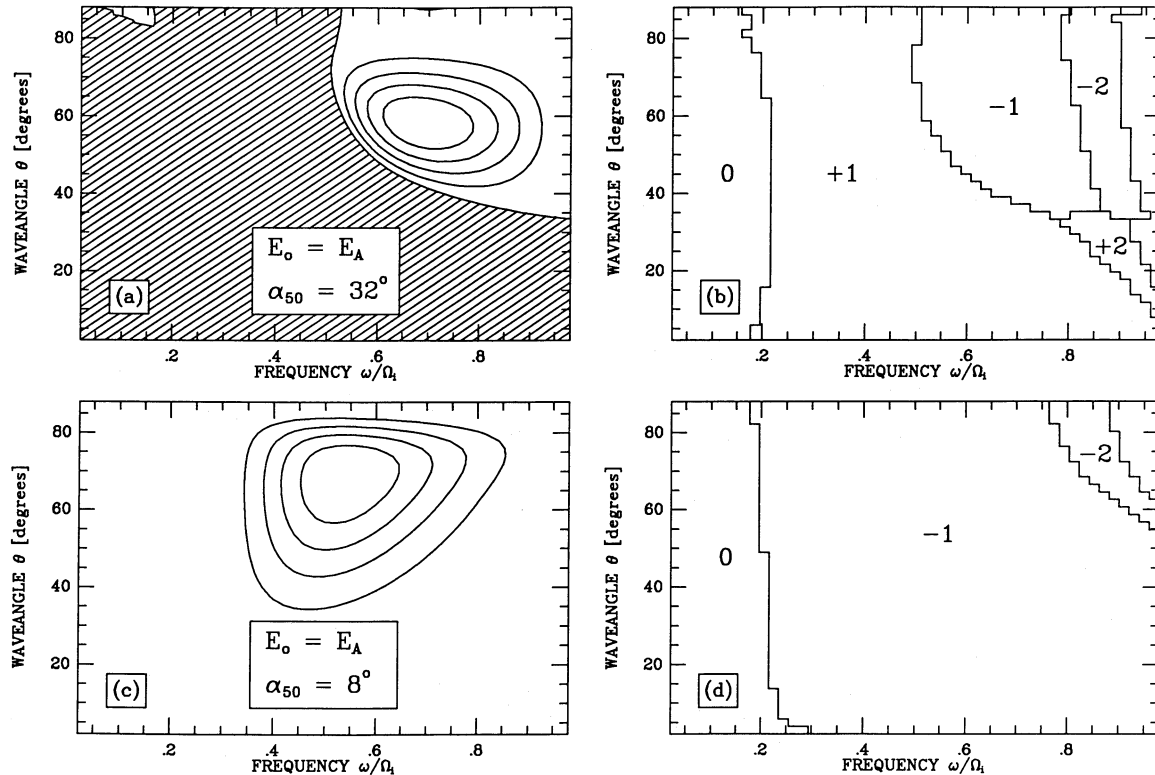


FIG. 1.—Contour maps of the absorption coefficient γ^σ corresponding to collimation angles $\alpha_{50} = 32^\circ$ (a) and $\alpha_{50} = 8^\circ$ (c) for the case $E_o = E_A$, where $E_o = m_p v_o^2/2$ and $E_A = m_p v_A^2/2$. In (b) (companion to [a]) and (d) (companion to [c]), boundaries enclose regions in which a particular harmonic (specified by the integer shown) tends to be the largest contributor to γ^σ . The smallest scale of serration in these boundaries indicates the resolution of the grid on which γ^σ is calculated: the grid spacing is 2° in θ and 0.02 units in ω/Ω_i , where Ω_i is the proton gyrofrequency. Only the harmonics $s = 0, \pm 1$, and ± 2 are mapped in (b) and (d). Hatched areas in the contour maps indicate the absence of wave growth. The four contour loops located in regions of wave growth, beginning with the outermost loop and progressing inward, correspond to γ^σ equal to 20%, 40%, 60%, and 80% of the maximum growth rate. (For the actual magnitude of the maximum growth rate, see Fig. 4.) The scale energy $E_o = m_p v_o^2/2$ for this case ($v_o = v_A$) equals 25 keV under the assumed conditions ($B = 10^2$ G, $n_i = 10^{10}$ cm $^{-3}$), placing it in the low range of the proton energies of interest (10–1000 keV).

of the wave parameters ω and θ is illustrated in Figures 1a, 1c, 2a, and 2c for selected values of the population parameters v_o and α_{50} . For Figure 1, v_o has been set equal to the Alfvén speed; for typical flare loop values of $B = 10^2$ G and $n_i = 10^{10}$ cm $^{-3}$, this sets the characteristic energy of the nonthermal protons to $m_p v_o^2/2 = 25$ keV. For Figure 2 the characteristic energy of the beam is larger by an order of magnitude ($v_o = 10^{1/2} v_A$).

A useful tool for understanding the patterns of wave growth is provided by the “dominant harmonic” map (see Figs. 1b, 1d, 2b, 2d, 3a, 3b), which identifies the harmonic tending to make the largest contribution to γ^σ in a given region of (ω, θ) space. Among the first features we notice in these maps is that the low frequency regime is dominated by the resonance at $s = 0$ (the so-called Cerenkov interaction). This is somewhat surprising because at low frequencies and at wave angles outside the immediate vicinity of $\theta = 0$ the Alfvén wave polarization is nearly linear, and linear polarization suppresses the $s = 0$ contribution to the absorption coefficient (to see this, observe that in the limit in which ψ , defined in equation (A3), goes to negative infinity, the right-side of equation (A4) vanishes). Why, then, does this harmonic dominate at low frequencies? As equation (6) shows, one must also consider the gradients of the distribution function $f(v)$ at the resonant parallel velocity $v_{\parallel} = (\omega - s\Omega_a)/k_{\parallel}$; at low frequency, where k_{\parallel} is small, the resonant parallel velocity for $s \neq 0$ lies far out in the tail of the distribu-

tion, where not only $f(v)$ but also the gradients of $f(v)$ are small. At sufficiently low frequency, these gradients are so weak that the $s = 0$ harmonic, although itself rather diminished by the polarization effect mentioned above, makes the major contribution to γ^σ . Due to the suppressing effect of wave polarization on the $s = 0$ term and of small gradients in $f(v)$ on the remaining terms, it is unlikely that the most vigorous wave growth can occur in the region of (ω, θ) space dominated by the resonance at $s = 0$. In fact, we find the maximum growth occurring consistently outside the $s = 0$ dominated region.

A further feature of the interaction at $s = 0$ is that it is completely unaffected by (i.e., receives zero contribution from) the perpendicular gradient of $f(v)$. As a consequence, it is decoupled from the general pattern of wave growth when the growth is driven primarily by $\partial f/\partial v_{\perp}$. This accounts for the topological disconnectedness of growth regions dominated by $s = 0$ from other growth regions in (ω, θ) space (see the unshaded area at the upper left of Fig. 1a). The contribution from the $s = 0$ term will be in the direction of wave growth or damping according to whether $\partial f/\partial v_{\parallel}$ is positive or negative, respectively, over the interval of v_{\perp} that contributes most to the integral in equation (6).

For the $s \neq 0$ harmonics it is instructive to consider how their relative contributions evolve from the fully isotropic case ($\alpha_{50} = 90^\circ$) to the strongly beamed case ($\alpha_{50} < 10^\circ$).

For the isotropic case, in which wave growth is entirely

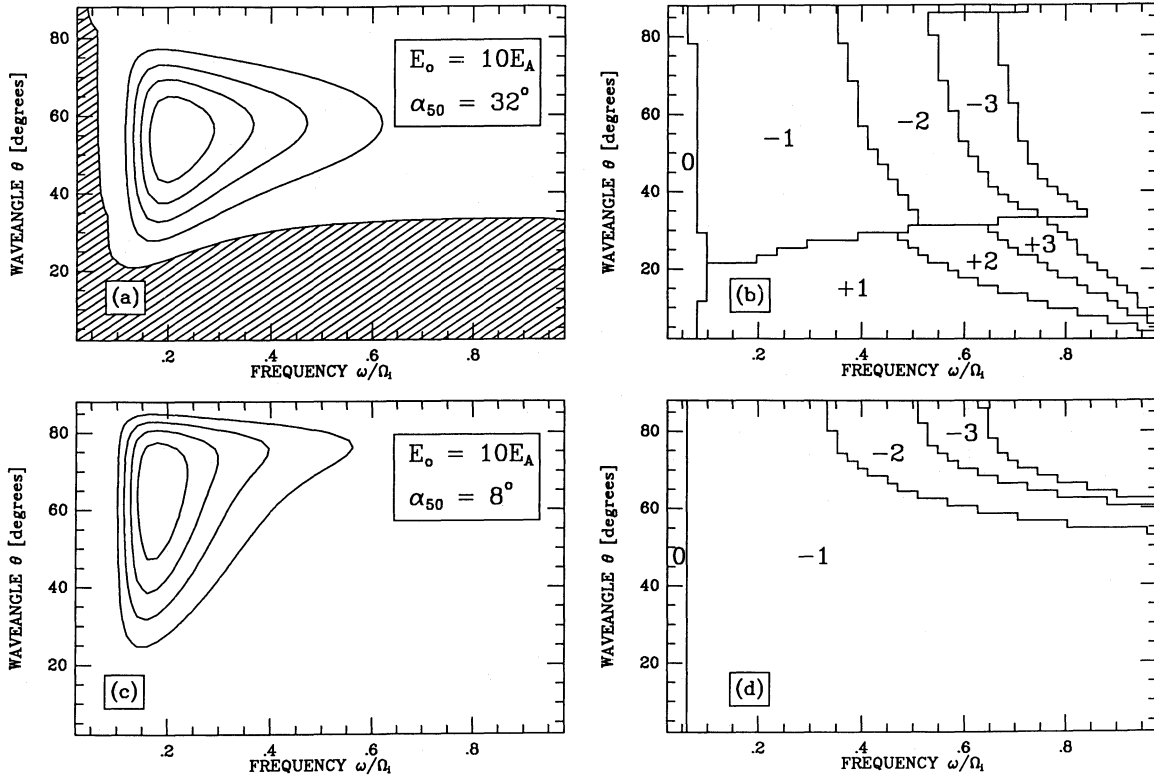


FIG. 2.—Same as Fig. 1, but for a beam that is one order of magnitude more energetic ($E_o = 10E_A$, equivalent to $v_o = 10^{1/2}v_A$). Figs. 2b and 2d extend to an additional harmonic order, $s = \pm 3$.

absent, the dominant harmonics are nonnegative (that is, $s \geq 0$) and appear to form a “band structure” in (ω, θ) space (Figs. 3a–3b). That the dominant harmonics in Figures 3a and 3b are nonnegative is partly due to the resonant parallel velocity $v_{\parallel} = (\omega - s\Omega_o)/k_{\parallel}$ lying systematically farther out in the tail of the distribution for negative harmonics as compared with the corresponding positive harmonics; that is, the bias toward nonnegative harmonics is gradient related. The band structure itself is linked to the ratio of the gyroradius v_{\perp}/Ω_o to the perpendicular wavelength k_{\perp}^{-1} of the resonant waves. When this ratio is small the higher order harmonics ($|s| \geq 2$) are unimportant. At larger wave frequencies and wave angles, where this ratio can be substantially larger than unity due to the decreased perpendicular wavelength, the Bessel functions appearing in the definition of $V(s, \mathbf{p}, \mathbf{k})$ allow other harmonics to exceed the importance of $|s| = 1$.

One notices that the band structure is narrower—that is, more closely spaced—in the case of the larger value of v_o considered (see Fig. 3b in comparison with Fig. 3a). Because the gyroradii are systematically larger for the higher energy beam, the bands appear at systematically larger values of the perpendicular wavelength. For a given wave angle, larger perpendicular wavelengths mean smaller frequencies, and it is precisely the systematic shifting of the edges of these bands to smaller frequencies that leads to the appearance of a more closely spaced structure.

Turning now to nonisotropic distributions, we see in Figures 1 and 2 that an increasingly greater area of (ω, θ) space is given to domination by negative harmonics ($s < 0$) as α_{50} decreases. A decrease in α_{50} yields a distribution that is more heavily weighted in the direction of the ambient magnetic field and is more collimated in pitch angle. Both of these trends act to

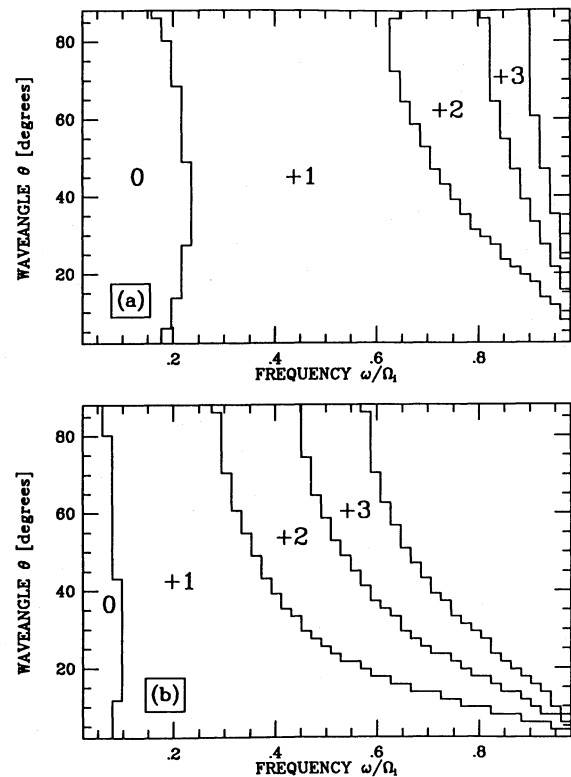


FIG. 3.—Maps of dominant harmonics—analogue to Figs. 1b, 1d, 2b, and 2d—for the isotropic case, $\alpha_{50} = 90^\circ$. The beam energies for Figs. 3a and 3b are $E_o = E_A$ and $E_o = 10E_A$, respectively. (The characteristic beam speeds for Figs. 3a and 3b are $v_o = v_A$ and $v_o = 10^{1/2}v_A$, respectively.)

increase the relative importance of the negative harmonics. The Doppler resonance condition indicates that protons having negative v_{\parallel} can be resonant with forward-propagating waves only at positive harmonics; as α_{50} decreases, the diminished fraction of protons that are characterized by negative v_{\parallel} helps to reduce the contribution from positive harmonics. Correspondingly, the magnitude of the negative harmonic contribution is enhanced by the increased fraction of forward-moving protons and is further enhanced by the stronger gradients found in the forward part of the proton distribution. Indeed, an important driver of wave growth for the streaming distribution is the steepening of the perpendicular gradient $\partial f/\partial v_{\perp}$ that accompanies the increased collimation of the beam. This (negative) gradient ensures that all negative harmonics contribute to wave growth through the term $(s\Omega_e/v_{\perp})\partial f/\partial v_{\perp}$ in equation (6). Among the negative harmonics, the resonance at $s = -1$ is expected to make the maximum contribution to wave growth, primarily because the resonant parallel velocity associated with $s = -1$ is the least distant on the tail of the nonthermal distribution function. We find that, indeed, the maximum wave growth occurs in the region of (ω, θ) space dominated by $s = -1$.

That wave growth is associated with negative harmonics is consistent with changes in particle momenta leading to a more relaxed distribution. Wave emission arising from resonant interaction results in a decrease in p_{\perp} in the amount $\hbar k_{\perp}$ together with a decrease in p_{\parallel} in the amount $\hbar k_{\parallel}$. Thus, emission of forward-propagating ($k_{\parallel} > 0$) waves via resonance at negative harmonics tends to relieve the excess in p_{\parallel} over p_{\perp} that characterizes a collimated streaming distribution.

Only as α_{50} is reduced to small values does domination by negative harmonics extend to small wave angles (see Figs. 1d and 2d). For the reasons just outlined, reduction in the value of α_{50} enhances the negative harmonics over the positive harmonics, gradually overcoming the initial domination by positive harmonics in the isotropic case. That this process happens first at large θ is a consequence of Alfvén wave polarization: the polarization-dependent coefficients (η_1, η_2 , and η_3 of eq. [A7])

introduce a weighting in favor of positive harmonics that is strongest in the range of smaller wave angles. The emergence of regions dominated by negative harmonics is thus conditioned on the overcoming of two biases: the polarization-related bias just mentioned as well as the gradient-related bias cited in our earlier discussion of the isotropic case.

To understand the polarization bias against negative harmonics at small wave angles, it is helpful to view the wave-proton interaction in the frame co-moving with the proton. Consider a parallel-propagating ($\theta = 0$) wave resonant with a proton at a negative harmonic ($s < 0$). In the co-moving frame, the wave electric field oscillates at a multiple of the proton gyrofrequency and is circularly polarized in a sense opposite to the gyromotion of the proton. Thus the time average of $\mathbf{E} \cdot \mathbf{j}$, where \mathbf{j} is the current associated with the proton's motion, vanishes and no power is transferred between particle and wave in the interaction. Power transfer at negative harmonics is relegated to oblique angles of wave propagation, but it is not obvious which specific value of the wave angle corresponds to maximum wave growth. A rough estimate can be obtained, however, by calculating the wave angle which maximizes the quantity $\eta_3 J_{s+1}^2(k_{\perp} v_{\perp}/\Omega_i)$ at the important $s = -1$ resonance. It suffices for this purpose to identify v_{\perp} in the argument of the Bessel function with v_o and to set the wave frequency to the value that satisfies the resonance condition $v_o = (\omega + \Omega_i)/k_{\parallel}(\omega, \theta = 0)$.

Figure 4 depicts the behavior of the maximum growth rate as the beam parameters are varied. For the purpose of depicting this behavior, we make use of the fact that the dependence of the growth rate on the beam-to-background proton density ratio n^*/n_i is one of direct proportionality [this follows from eq. [6] where $f_d(v)$ contributes a factor of n^* , and $R_E^{\sigma}(k)$ contributes a factor of n_i^{-1} via its dependence on v_A^2/c^2 (eq. [A1])]. This enables us to define a dimensionless quantity G according to the relation $|\gamma^{\sigma}|_{\max} = \Omega_i(n^*/n_i)G$, where G is a function only of v_o and α_{50} . Figure 4 shows, not surprisingly, that G rises monotonically with decreasing α_{50} . It shows also that, over the range of α_{50} considered, G remains within an order of magni-

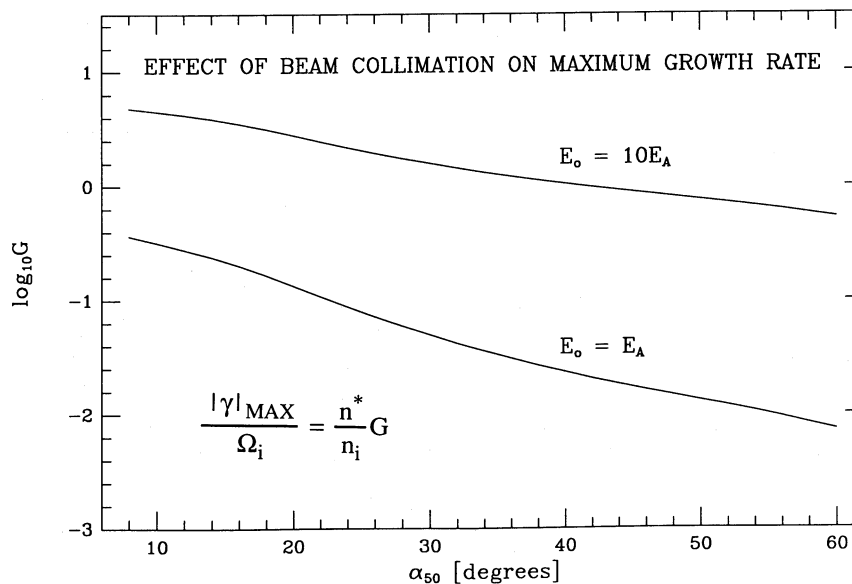


FIG. 4.—Effect of α_{50} on the parameter G , defined here to be the factor which multiplies the beam-to-background proton density ratio n^*/n_i to yield the maximum wave growth rate in units of the proton gyrofrequency. The variation of G with respect to α_{50} is shown for the two characteristic beam energies considered in Figs. 1 and 2.

tude of unity for the higher energy beam considered ($v_o = 10^{1/2}v_A$). In comparison with the value of G for the higher energy beam, the value of G for the lower energy beam ($v_o = v_A$) ranges from one order of magnitude less (at $\alpha_{50} \approx 10^\circ$) to two orders of magnitude less (at $\alpha_{50} \approx 60^\circ$). Underlying the tendency for G to be systematically greater for the higher energy beam is a kinematic result: at larger values of v_{\parallel} , resonance at the important harmonic ($s = -1$) involves Alfvén waves of lower frequency. For the higher energy beam, this systematically enhances G through the lower frequency that one uses in evaluating the coefficient $R_G^2(k)/(\omega^\sigma(k)|k_{\parallel}|)$ that appears to the left of the summation in equation (6). Finally, we note that the maximum wave growth occurs at relatively large wave angles (Figs. 1 and 2), a consequence of the polarization bias mentioned above. It is worth pointing out that this bias works in the opposite sense for the magnetoacoustic mode, tending to favor negative over positive harmonics at small wave angles. This suggests that the magnetoacoustic mode, by allowing the streaming distribution to shed excess forward momentum efficiently via the forward emission of parallel-propagating waves, may exhibit larger overall growth rates.

b) Thermal Damping and its Effect on Beam Stability in the Flare Loop

For mathematical convenience, the distribution function describing the protons in the system has been decomposed into the sum of two functions. The first, describing the nonthermal population, has been specified in equation (7) and its contribution to the absorption coefficient γ^σ discussed in the preceding section. The second, which describes the thermal proton population, is assumed to be an isotropic Maxwellian whose characteristic speed is the proton thermal speed, $V_i = (kT_i/m_p)^{1/2}$. Let us denote by $\gamma_i(\omega, \theta, T_i)$ the contribution to the absorption coefficient from the thermal proton population (the contribution from thermal electrons to the growth or damping of Alfvén waves is small in comparison with that from thermal protons when $T_e = T_i$). Noting that the contribution to the absorption coefficient from the nonthermal proton population is directly proportional to the beam-to-background proton density ratio n^*/n_i as pointed out above, we may conveniently represent the net absorption coefficient due to the system protons by the following relation:

$$\gamma(\omega, \theta, v_o, \alpha_{50}, T_i, n^*/n_i) = \frac{n^*}{n_i} \gamma_n(\omega, \theta, v_o, \alpha_{50}) + \gamma_i(\omega, \theta, T_i) \quad (9)$$

where $\gamma_n(\omega, \theta, v_o, \alpha_{50})$ is the contribution from the nonthermal proton population apart from the factor of n^*/n_i . The thermal term $\gamma_i(\omega, \theta, T_i)$ is positive definite (damping) and therefore competes with the (negative) nonthermal term $\gamma_n(\omega, \theta, v_o, \alpha_{50})$ when the latter favors wave growth. In these circumstances, it is the beam-to-background proton density ratio which ultimately determines the sign of the net absorption coefficient.

For chosen values of T_i , n^*/n_i , v_o , and α_{50} , the maximum net growth rate is obtained by scanning (ω, θ) space for the most negative value of the net absorption coefficient. Let us denote the maximum net growth rate by γ_{\max} and the location at which it occurs in (ω, θ) space by (ω_m, θ_m) . The ratio $v_{g\parallel}/|\gamma_{\max}|$, where $v_{g\parallel}$ is the parallel component of the group velocity evaluated at (ω_m, θ_m) , is the length scale associated with a single e -folding of energy density of the most vigorously growing

waves. A single e -folding, however, corresponds to a relatively modest increase in wave energy density. We are interested in wave energy densities sufficiently large to cause effective particle scattering, therefore an appropriate length scale for characterizing effective wave growth is $L_G = 10 v_{g\parallel}/|\gamma_{\max}|$, i.e., one order of magnitude larger than the single e -folding scale. We define "beam stability" in the present context as the condition $L_G > L$, where L is the loop semilength. By contrast, a condition of effective scattering of the beam ("beam instability") is said to exist if $L_G < L$.

The boundary in parameter space between the regions of effective scattering (beam instability) and ineffective scattering (beam stability) is specified by the equation $L_G = L$. If v_o , L , and T_i are considered constant, the equation $L_G = L$ becomes an implicit equation for n^*/n_i as a function of α_{50} . The relation between these two variables is shown in Figures 5 and 6, where one sees, as one might expect, that the threshold value of the beam-to-background proton density ratio n^*/n_i generally decreases as the beam collimation angle narrows.

Figures 5 and 6 also illustrate the effect of thermal damping on beam stability. For the case $v_o = v_A$ (Fig. 5), intended to represent a deka-keV proton beam, temperatures on the order of 5 million K, which are quite plausible for the flaring coronal loop, have the effect of raising significantly the threshold beam-to-background proton density ratio for beams of moderate collimation ($\alpha_{50} \gtrsim 40^\circ$). For the case of $v_o = 10^{1/2}v_A$ (Fig. 6), intended to represent a proton beam of hundreds of keV, higher temperatures are needed to achieve notable thermal damping effects, the reason being that higher temperatures provide a greater abundance of fast protons in the tail of the thermal Maxwellian that can be resonant with the lower frequency waves which the higher energy beam drives to growth. At 30 million K, for example, the threshold values of n^*/n_i depicted in Figure 6 are not greatly different from the zero temperature case. At collimation angles as large as 60° , even a temperature of 50 million K, already in the upper range of temperatures seen in solar flares, is insufficient to raise the threshold value of n^*/n_i above 2×10^{-5} .

We caution that Figure 5 must not be taken to imply that arbitrarily intense proton beams may be stabilized by thermal damping. The formalism on which Figure 5 is based assumes that n^*/n_i is sufficiently small to ensure that $|\gamma^\sigma|/\omega \ll 1$. For the case under discussion, this precludes consideration of n^*/n_i exceeding $\sim 10^{-2}$. The beam energy flux associated with $n^*/n_i = 10^{-2}$ for the case $v_o = v_A$ can be estimated to order of magnitude from the expression $(m_p v_o^2/2)n^*v_o$; under the assumed conditions, one finds the energy flux to lie in the range 10^8 – 10^9 ergs $\text{cm}^{-2} \text{s}^{-1}$. Larger beam energy fluxes may excite a nonresonant instability (the firehose instability).

In order for scattering to be effective, there is an additional requirement that waves not leak out the sides of the flux tube before they can be driven to large amplitude. If R represents the flux tube radius and L the loop semi-length, then the condition for leakage to be unimportant is $v_{g\perp}/v_{g\parallel} < R/L$, where $v_{g\perp}$ and $v_{g\parallel}$ are, respectively, the perpendicular and parallel components of the group velocity of the relevant waves. The aspect ratio R/L may be estimated from soft X-ray and ultraviolet images of loops (Webb 1981; Eddy 1979); reasonable estimates place R/L in the range 1/5 to 1/10. Straightforward evaluation of the ratio $v_{g\perp}/v_{g\parallel}$ for the most vigorously growing waves yields values consistently below this estimated range of R/L . Leakage is therefore not likely by itself to prevent the growth of the resonant instability.

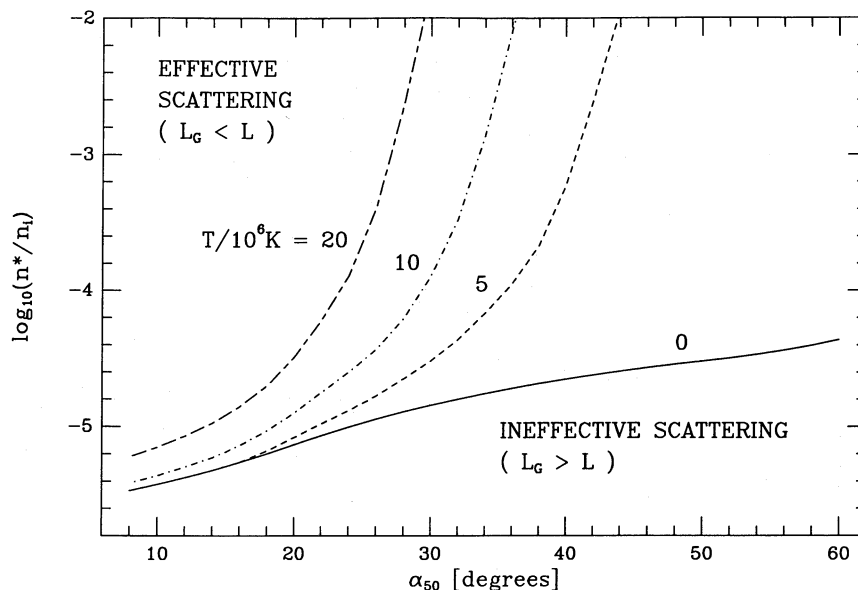


FIG. 5.—Curves of $L_G = L$, where L_G is the length scale for effective wave growth and L is the loop semilength, for the case $v_o = v_A$. We assume $L = 10^9$ cm, $B = 10^2$ G, and $n_i = 10^{10}$ cm $^{-3}$. Thermal damping, arising from wave resonance with the background plasma, is explicitly included in the calculation of L_G . Four values of the background temperature are considered. To the right of a given curve lies the region of effective beam stability ($L_G > L$), and to the left lies the region of effective beam instability ($L_G < L$), in the flare loop context.

IV. CONCLUSIONS

We have investigated the growth of Alfvén waves in magnetized hydrogen plasma at flare-loop densities and magnetic field strengths driven by a dilute population of streaming protons in the energy range 10–1000 keV. Our conclusions fall into three categories: those relating to the dependence of the growth rate on frequency and wave angle, those bearing on the maximum growth rate, and those concerning the stability of the proton distribution in solar flare loops.

Concerning the patterns of wave growth we find the following.

1. The streaming distribution induces wave growth prin-

cipally through resonant interactions between forward-moving protons and forward-propagating waves.

2. The most vigorous wave growth occurs via the harmonic $s = -1$.

3. The area of (ω, θ) space given to wave growth expands with narrower beam collimation.

4. For Alfvén waves of sufficiently low frequency the dominant interaction is via the $s = 0$ harmonic. As a consequence, the tendency toward growth of the lowest frequency waves is determined, not by the perpendicular gradient in the beam's distribution function (which drives the most vigorous wave growth via the $s = -1$ resonance), but rather by the parallel gradient.

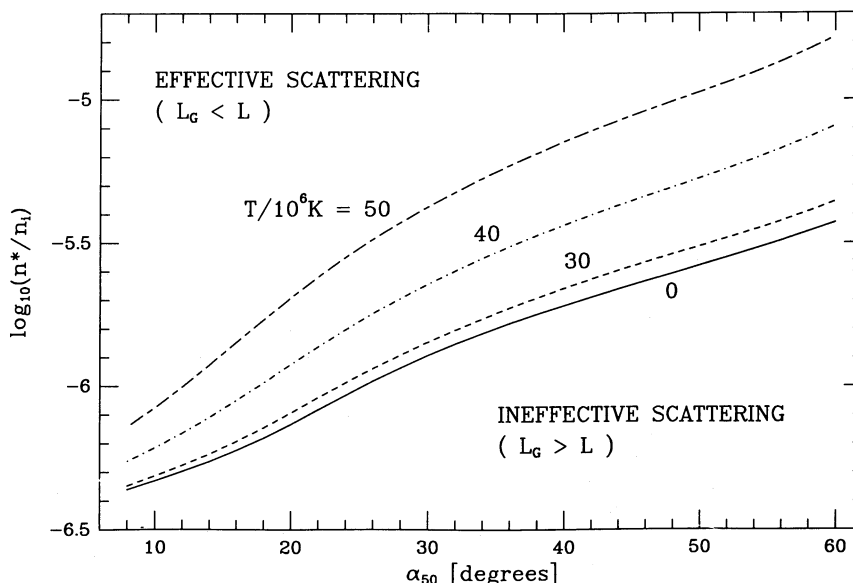


FIG. 6.—Same as Fig. 5, but for a beam that is one order of magnitude more energetic ($v_o = 10^{1/2}v_A$)

We note the following behaviors in the maximum growth rate

1. All other factors constant, the maximum growth rate increases with mean beam energy and with increased narrowness (i.e., decreased α_{50}) of the beam distribution.

2. The frequency of the most rapidly growing waves is inversely related to the mean beam energy.

3. The waves exhibiting the most vigorous growth have large ($\theta > 50^\circ$) wave angles; their group velocity, however, remains nearly parallel to the magnetic field.

Vigorous Alfvén wave growth induced by streaming protons in the solar flare loop can lead to effective resonant scattering and thus rapid isotropization of the protons. We have estimated the conditions for this to occur by comparing the wave growth length scale L_G to the loop semilength L . Defining "beam stability" in this context as the condition $L_G > L$, we find that for typical flare loop parameters ($B = 10^2$ G, $L = 10^9$

cm, $n_i = 10^{10}$ cm $^{-3}$, temperatures of a few million K) a dilute ($n^*/n_i < 10^{-2}$) proton beam of deka-keV mean energy ($v_o = v_A$) and moderate collimation ($\alpha_{50} \gtrsim 40^\circ$) is rendered stable by thermal damping. However, for a similarly collimated beam only one order of magnitude more energetic, thermal damping at the expected prevailing temperatures is insufficient to quench the induced wave growth, rendering stability contingent upon extreme diluteness of the beam. We conclude that streaming instabilities begin to pose a significant constraint on the sustained propagation of directed proton streams in solar flare loops at mean beam energies that are only a small multiple of $m_p v_A^2/2$.

This work has been supported by the National Aeronautics and Space Administration through grant NAGW-864 and by the National Science Foundation through grants ATM 85-96006 and ATM 86-19853.

APPENDIX

SOME PROPERTIES OF THE ALFVÉN WAVE

Following the standard methods (Melrose 1980), with the dispersion relation as given in equation (5), one obtains the following expression for the ratio of electric energy density to total energy density in the Alfvén wave:

$$R_E^\sigma(\mathbf{k}) = \frac{v_A^2}{c^2} \left(\frac{1 + \psi^2}{1 + \psi^2 \cos^2 \theta} \right) \frac{(1 - \chi^2)^2 (\tan^4 \theta + 4\chi^2 \sec^2 \theta)^{1/2}}{[(1 + \sec^2 \theta)(\tan^4 \theta + 4\chi^2 \sec^2 \theta)^{1/2} + \tan^4 \theta + 2\chi^2(3 - \chi^2) \sec^2 \theta]}, \quad (\text{A1})$$

where χ denotes ω/Ω_i and ψ is defined in equation (A3) below. The quantity $R_E^\sigma(\mathbf{k})$ equals $v_A^2/(2c^2)$ at low frequency and falls monotonically to zero as χ approaches unity. It depends only weakly on the wave angle θ .

The standard methods also yield the following for the complex electric polarization unit vector of the Alfvén wave, represented here in the same coordinate system as has been used to represent $V(s, \mathbf{p}, \mathbf{k})$ in equation (3):

$$\hat{e}^\sigma(\mathbf{k}) = \frac{1}{(\psi^2 + 1)^{1/2}} (\psi, i, 0), \quad (\text{A2})$$

where

$$\psi = -\frac{1}{2\chi} [\tan^2 \theta + (\tan^4 \theta + 4\chi^2 \sec^2 \theta)^{1/2}]. \quad (\text{A3})$$

It follows that

$$|\hat{e}^{\sigma*}(\mathbf{k}) \cdot V(s, \mathbf{p}, \mathbf{k})|^2 = v_\perp^2 [\eta_1 J_{s-1}^2(\zeta_a) + \eta_2 J_{s-1}(\zeta_a) J_{s+1}(\zeta_a) + \eta_3 J_{s+1}^2(\zeta_a)], \quad (\text{A4})$$

where $\zeta_a = k_\perp v_\perp / \Omega_a$, and where we have used the following two recursion formulae for Bessel functions

$$\frac{2s}{z} J_s(z) = J_{s-1}(z) + J_{s+1}(z), \quad (\text{A5})$$

$$2J'_s(z) = J_{s-1}(z) - J_{s+1}(z), \quad (\text{A6})$$

and have defined the coefficients η_1 , η_2 , and η_3 as follows:

$$\eta_1 = \frac{(\psi - \epsilon_a)^2}{4(\psi^2 + 1)}, \quad \eta_2 = \frac{\psi^2 - 1}{2(\psi^2 + 1)}, \quad \eta_3 = \frac{(\psi + \epsilon_a)^2}{4(\psi^2 + 1)}. \quad (\text{A7})$$

Here, ϵ_a denotes $q_a/|q_a|$, where q_a is the electric charge of the particle species interacting with the waves. For the case of Alfvén waves interacting with proton ($\epsilon_a = +1$), both η_2 and η_3 are small in comparison with η_1 as the direction of wave propagation approaches the direction parallel to the background magnetic field (that is, as ψ approaches -1).

When the interaction is between Alfvén waves and the streaming distribution of protons described by equation (7), the expression for the absorption coefficient γ^σ (eq. [6]) leads to integrals of the form

$$\int_0^\infty x^{s+1} e^{-\mu x^2} J_{s-n}(\zeta x) J_{s+n}(\zeta x) dx, \quad |s| \geq n \geq 0. \quad (\text{A8})$$

With aid from Gradshteyn and Ryzhik (1980) one can show that this integral, which is convergent and positive definite for all

integer s , has a series solution given by

$$\frac{1}{2} \left(\frac{\xi}{2}\right)^{2|s|} \mu^{-(|s|+\Lambda+1)} \sum_{m=0}^{\infty} a_m \left(\frac{-\xi^2}{2\mu}\right)^m, \quad (\text{A9})$$

where $\Lambda = \lambda/2$ and where the series coefficient is given by

$$a_m = \frac{\Gamma(m+1+|s|+\Lambda)\Gamma(2m+1+2|s|)}{\Gamma(m+1)\Gamma(m+1+|s|-n)\Gamma(m+1+|s|+n)\Gamma(m+1+2|s|)}. \quad (\text{A10})$$

REFERENCES

- Benz, A. O., and Simnett, G. M. 1986, *Nature*, **320**, 508.
 Canfield, R. C., and Chang, C.-R. 1985, *Ap. J.*, **295**, 275.
 Chupp, E. L. 1984, *Ann Rev. Astr. Ap.*, **22**, 359.
 Chupp, E. L., Forrest, D. J., Higbie, P. R., Suri, A. N., Tsai, C., and Dunphy, P. P. 1973, *Nature*, **241**, 333.
 Eddy, J. A. 1979, *A New Sun: The Solar Results from Skylab* (Washington: NASA SP-402).
 Forman, M. A., Ramaty, R., and Zweibel, E. G. 1986, in *Physics of the Sun*, Vol. 2, ed. P. A. Sturrock, T. E. Holzer, D. M. Mihalas, and R. K. Ulrich (Dordrecht: Reidel), p. 249.
 Gradshteyn, I. S., and Ryzhik, I. M. 1980, *Table of Integrals, Series, and Products* (New York: Academic).
 McClements, K. G. 1987, *Solar Phys.*, **109**, 355.
 Melrose, D. B. 1980, *Plasma Astrophysics*, Vols. 1-2 (New York: Gordon & Breach).
 Melrose, D. B. 1986, *Instabilities in Space and Laboratory Plasmas* (Cambridge: Cambridge University Press).
 Mok, Y. 1985, *Solar Phys.*, **95**, 181.
 Orrall, F. Q., and Zirker, J. B. 1976, *Ap. J.*, **208**, 618.
 Press, W. H., Flannery, B. P., Teukolsky, S. A., and Vetterling, W. T. 1986, *Numerical Recipes* (Cambridge: Cambridge University Press).
 Ramaty, R., Kozlovsky, B., and Lingenfelter, R. E. 1975, *Space Sci. Rev.*, **18**, 341.
 Sarris, E. T., and Krimigis, S. M. 1985, *Solar Phys.*, **96**, 413.
 Stix, T. H. 1962, *The Theory of Plasma Waves* (New York: McGraw-Hill).
 Tamres, D. H., Canfield, R. C., and McClymont, A. N. 1986, *Ap. J.*, **309**, 409.
 Webb, D. F. 1981, in *Solar Active Regions: A Monograph from Skylab Solar Workshop III*, ed. F. Q. Orrall (Boulder, Colorado: Colorado Associated University Press), p. 165.

R. C. CANFIELD and D. H. TAMRES: Institute for Astronomy, University of Hawaii, 2680 Woodlawn Drive, Honolulu, HI 96822

D. B. MELROSE: School of Physics, University of Sydney, Sydney NSW 2006, Australia